Received 12 February; accepted 16 March 2004; doi:10.1038/nature02505.

1. Bos, J. L., de Rooij, J. & Reedquist, K. A. Rap1 signalling: adhering to new models. *Nature Rev. Mol. Cell. Biol.* **2,** 369–377 (2001).
2. Hattori, M. & Minato, N. Rap1 GTPase: functions, regulation, and malignancy. *J. Biochem. (Tokyo)* **134,** 479–484 (2003).
3. Vetter, I. R. & Wittinghofer, A. The guanine nucleotide-binding switch in three dimensions. *Science* **294,** 1299–1304 (2001).
4. Brinkmann, T. *et al.* Rap-specific GTPase activating protein follows an alternative mechanism. *J Biol. Chem.* **277,** 12525–12531 (2002).
5. Rubinfeld, B. *et al.* Molecular cloning of a GTPase activating protein specific for the Krev-1 protein p21rap1. *Cell* **65,** 1033–1042 (1991).
6. Rubinfeld, B. *et al.* Localisation of the rap1GAP catalytic domain and sites of phosphorylation by mutational analysis. *Mol. Cell. Biol.* **12,** 4634–4642 (1992).
7. Hattori, M. *et al.* Molecular cloning of a novel mitogen-inducible nuclear protein with a Ran GTPase-activating domain that affects cell cycle progression. *Mol Cell. Biol.* **15,** 552–560 (1995).
8. Gao, Q., Srinivasan, S., Boyer, S. N., Wazer, D. E. & Band, V. The E6 oncoproteins of high-risk papillomaviruses bind to a novel putative GAP protein, E6TP1, and target it for degradation. *Mol. Cell. Biol.* **19,** 733–744 (1999).
9. Manning, B. D. & Cantley, L. C. Rheb fills a GAP between TSC and TOR. *Trends Biochem. Sci.* **28,** 573–576 (2003).
10. Gao, Q. *et al.* Human papillomavirus type 16 E6-induced degradation of E6TP1 correlates with its ability to immortalise human mammary epithelial cells. *J. Virol.* **75,** 4459–4466 (2001).
11. Ishida, D. *et al.* Myeloproliferative stem cell disorders by deregulated Rap1 activation in SPA-1-deficient mice. *Cancer Cell* **4,** 55–65 (2003).
12. Kraemer, A., Brinkmann, T., Plettner, I., Goody, R. & Wittinghofer, A. Fluorescently labelled guanine nucleotide binding proteins to analyse elementary steps of GAP-catalysed reactions. *J. Mol. Biol.* **324,** 763–774 (2002).
13. Chabre, M. Aluminofluoride and beryllofluoride complexes: a new phosphate analogs in enzymology. *Trends Biochem. Sci.* **15,** 6–10 (1990).
14. Scheffzek, K., Ahmadian, M. R. & Wittinghofer, A. GTPase-activating proteins: helping hands to complement an active site. *Trends Biochem. Sci.* **23,** 257–262 (1998).
15. Maheshwar, M. M. *et al.* The GAP-related domain of tuberin, the product of the TSC2 gene, is a target for missense mutations in tuberous sclerosis. *Hum. Mol. Genet.* **6,** 1991–1996 (1997).
16. Jones, A. C. *et al.* Comprehensive mutation analysis of TSC1 and TSC2 and phenotypic correlations in 150 families with tuberous sclerosis. *Am. J. Hum. Genet.* **64,** 1305–1315 (1999).
17. Au, K. S. *et al.* Germ-line mutational analysis of the TSC2 gene in 90 tuberous-sclerosis patients. *Am. J. Hum. Genet.* **62,** 286–294 (1998).
18. Klose, A. *et al.* Selective disactivation of neurofibromin GAP activity in neurofibromatosis type 1. *Hum. Mol. Genet.* **7,** 1261–1268 (1998).
19. Xu, X., Wang, Y., Barry, D. C., Chanock, S. J. & Bokoch, G. M. Guanine nucleotide binding properties of Rac2 mutant proteins and analysis of the responsiveness to guanine nucleotide dissociation stimulator. *Biochemistry* **36,** 626–632 (1997).
20. Seewald, M. J., Körner, C., Wittinghofer, A. & Vetter, I. R. RanGAP mediates GTP hydrolysis without an arginine finger. *Nature* **415,** 662–666 (2002).
21. De Antoni, A., Schmitzova, J., Trepte, H. H., Gallwitz, D. & Albert, S. Significance of GTP hydrolysis in Ypt1p-regulated endoplasmic reticulum to Golgi transport revealed by the analysis of two novel Ypt1-GAPs. *J. Biol. Chem.* **277,** 41023–41031 (2002).
22. Ahmadian, M. R., Stege, P., Scheffzek, K. & Wittinghofer, A. Confirmation of the arginine-finger hypothesis for the GAP-stimulated GTP-hydrolysis reaction of Ras. *Nature Struct. Biol.* **4,** 686–689 (1997).
23. Albert, S., Will, E. & Gallwitz, D. Identification of the catalytic domains and their functionally critical arginine residues of two yeast GTPase-activating proteins specific for Ypt/Rab transport GTPases. *EMBO J.* **18,** 5216–5225 (1999).
24. Nassar, N., Hoffman, G. R., Manor, D., Clardy, J. C. & Cerione, R. A. Structures of Cdc42 bound to the active and catalytically compromised forms of Cdc42GAP. *Nature Struct. Biol.* **5,** 1047–1052 (1998).
25. Graham, D. L., Eccleston, J. F., Chung, C. W. & Lowe, P. N. Magnesium fluoride-dependent binding of small G proteins to their GTPase-activating proteins. *Biochemistry* **38,** 14981–14987 (1999).
26. Goldberg, J. Structural and functional analysis of the ARF1-ARFGAP complex reveals a role for coatomer in GTP hydrolysis. *Cell* **96,** 893–902 (1999).
27. Scheffzek, K. *et al.* The Ras-RasGAP complex: structural basis for GTPase activation and its loss in oncogenic Ras mutants. *Science* **277,** 333–338 (1997).
28. Rittinger, K., Walker, P. A., Eccleston, J. F., Smerdon, S. J. & Gamblin, S. J. Structure at 1.65 Å of RhoA and its GTPase-activating protein in complex with a transition-state analogue. *Nature* **389,** 758–762 (1997).
29. Daumke, O., Wittinghofer, A. & Weyand, M. Purification, crystallisation and preliminary structural characterisation of human Rap1GAP. *Acta Crystallogr. D* **60,** 752–754 (2004).
30. Lenzen, C., Cool, R. H. & Wittinghofer, A. Analysis of intrinsic and CDC25-stimulated guanine nucleotide exchange of p21ras-nucleotide complexes by fluorescence measurements. *Methods Enzymol.* **255,** 95–109 (1995).

Supplementary Information accompanies the paper on **www.nature.com/nature**.

Acknowledgements We thank A. Krämer for the gift of Rap1-Aedans·GTP. We thank I. Schlichting, W. Blankenfeldt, A. Scheidig, A. Rak, E. Wolf and O. Yildiz for data collection and crystallographic advice and the ESRF beam staff of beamline ID14-1 in Grenoble for support. O.D. thanks the Boehringer Ingelheim Fonds and P.P.C. the International Max-Planck Research School for support.

Competing interests statement The authors declare that they have no competing financial interests.

Correspondence and requests for materials should be addressed to A.W. (alfred.wittinghofer@mpi-dortmund.mpg.de). Coordinates have been deposited to the Protein Data Bank under accession code 1SRQ.

A conformational switch controls hepatitis delta virus ribozyme catalysis

Ailong Ke[1], Kaihong Zhou[2], Fang Ding[1], Jamie H. D. Cate[1] & Jennifer A. Doudna[1,2]

[1]*Department of Molecular and Cell Biology and Department of Chemistry, and* [2]*Howard Hughes Medical Institute, University of California at Berkeley, Berkeley, California 94705, USA*

Ribozymes enhance chemical reaction rates using many of the same catalytic strategies as protein enzymes. In the hepatitis delta virus (HDV) ribozyme, site-specific self-cleavage of the viral RNA phosphodiester backbone[1–3] requires both divalent cations and a cytidine nucleotide[4–6]. General acid–base catalysis[7–12], substrate destabilization[1,13] and global and local conformational changes[14,15] have all been proposed to contribute to the ribozyme catalytic mechanism. Here we report ten crystal structures of the HDV ribozyme in its pre-cleaved state, showing that cytidine is positioned to activate the 2′-OH nucleophile in the precursor structure. This observation supports its proposed role as a general base in the reaction mechanism. Comparison of crystal structures of the ribozyme in the pre- and post-cleavage states reveals a significant conformational change in the RNA after cleavage and that a catalytically critical divalent metal ion from the active site is ejected. The HDV ribozyme has remarkable chemical similarity to protein ribonucleases and to zymogens for which conformational dynamics are integral to biological activity. This finding implies that RNA structural rearrangements control the reactivity of ribozymes and ribonucleoprotein enzymes.

To elucidate the catalytic mechanism used by the HDV ribozyme, we determined ten crystal structures of precursor forms of the ribozyme in which catalysis was prevented by mutation of the catalytically essential cytidine 75, chelation of divalent metal ions or 2′-deoxy substitution of the 2′-OH nucleophile (see Supplementary Table S1). Structures of the C75U mutant ribozyme and the wild-type genomic precursor ribozyme were solved at resolutions up to 2.2 Å and 3.4 Å, respectively. In all cases the structure of the precursor ribozyme resembles that of the product in overall conformation (Fig. 1a, b). The electron density at the active site of the C75U mutant reveals that the substrate RNA strand preceding the cleavage site makes a sharp ~180° turn about the scissile phosphate between the G1 and U −1 bases, packing the substrate strand into the P1 major groove and possibly destabilizing it in the ground state[13] (Fig. 1c). Only the sugar–phosphate backbone density is visible preceding the scissile phosphate, and there appears to be no strong interaction between the substrate bases and the rest of the ribozyme, consistent with the low sequence preference 5′ to the cleavage site[16,17].

In contrast to the structure of the product form of the HDV ribozyme[7], electron density for a divalent cation coordinated to the 5′ leaving oxygen is observed in the precursor ribozyme structures (Fig. 1c). Although the position of the active site metal ion varies slightly in the C75U mutant structures, in all cases it binds by outer-sphere coordination to six functional groups (four phosphoryl oxygen and two uracil keto oxygen atoms) that form a pocket adjacent to the scissile bond (Fig. 1d; Supplementary Fig. S1). Interestingly, the wild-type HDV ribozyme that was prepared and crystallized in the absence of divalent metal ions has the same structure as that observed for the C75U mutant precursor (r.m.s.d. of 0.30 Å for all-phosphorus-atom superposition), yet lacks any trace of the metal ion in the active-site metal-binding pocket

(Fig. 2a). This observation rules out disruption of active site geometry by the C75U mutation and shows that divalent metal ions are not required for HDV ribozyme folding, in contrast to some other ribozymes (reviewed in ref. 18).

To investigate whether the divalent cation observed in the active site participates directly in catalysis, we first showed that, consistent with previous results[4,5], the ribozyme is active in the presence of a wide spectrum of metal ions, including Mg^{2+}, Ca^{2+}, Sr^{2+}, Ba^{2+}, Mn^{2+} and Co^{2+}. It has trace activity in Cd^{2+} and Ni^{2+} solutions, no activity in the presence of Cu^{2+} and is specifically inhibited by $Co(NH_3)_6^{3+}$ (data not shown). To test the correlation between activity and metal-ion binding, various divalent cations including Mg^{2+}, Sr^{2+}, Ba^{2+} and Mn^{2+} were introduced into the C75U ribozyme crystals and shown to be present in the active site in difference and anomalous difference electron-density maps (Supplementary Table S1). By contrast, Cu^{2+}, a cation that fails to support HDV ribozyme cleavage, does not bind in the active site. Furthermore, the inhibitory cations $Co(NH_3)_6^{3+}$ and $Ir(NH_3)_6^{3+}$ occupy the same site as the divalent ion and produce strong anomalous diffraction signals even after soaking crystals in 0.5–1 mM hexammine in the presence of 20 mM competing Mg^{2+} or Sr^{2+}. $Co(NH_3)_6^{3+}$ is also a competitive inhibitor of imidazole-catalysed cleavage of the C75U mutant ribozyme (Supplementary Fig. S2). Together, these data show a strict correlation between the activity of the ribozyme and the presence of a hydrated divalent cation at the active site. Importantly, a divalent ion binds similarly in the active site of a wild-type precursor ribozyme, as revealed in a difference electron-density map comparing structures of this ribo-

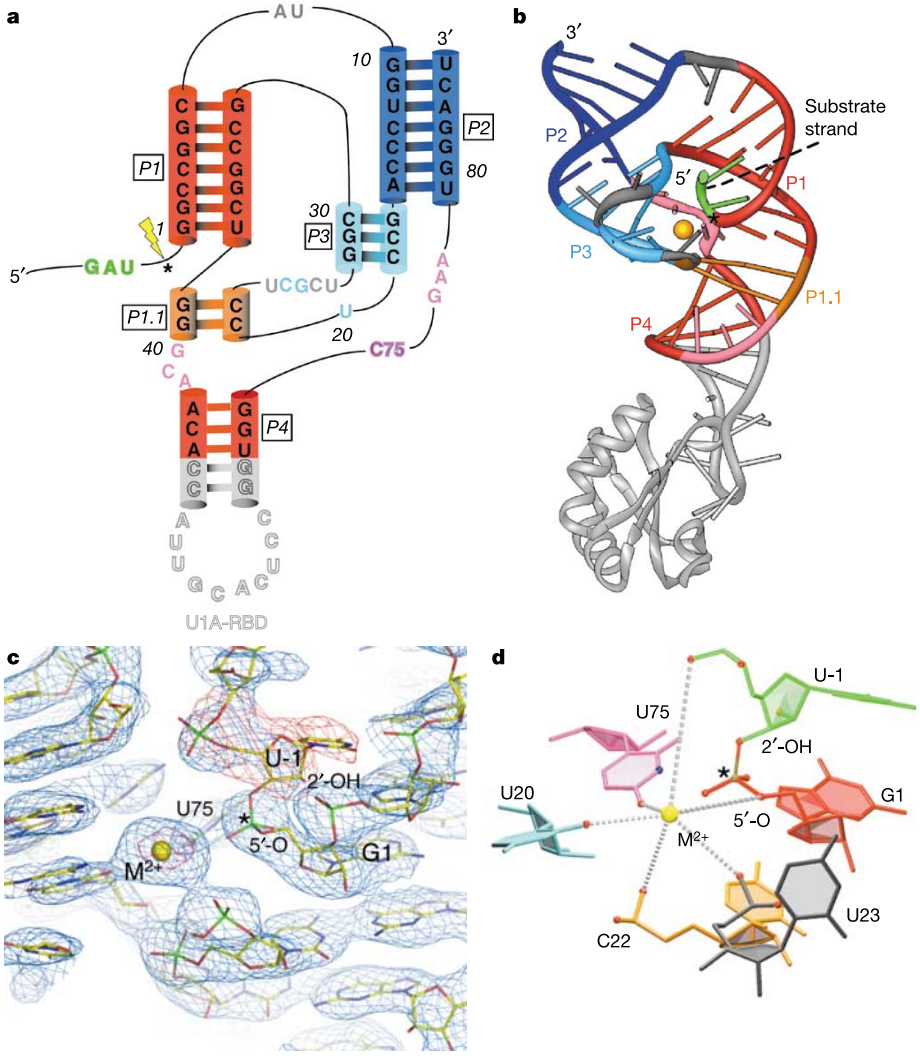

Figure 1 Precursor HDV ribozyme crystal structure. **a**, Sequence and secondary structure of the precursor-form HDV ribozyme crystallization constructs. Structural element colours match the three-dimensional representation in subsequent figures: substrate strand, green; P1, P4, red; J1/2, L3, grey; P2, blue; P3, light blue; J1.1/4, J4/2, pink; P1.1, orange; U1A-RBD and binding site, silver. Scissile phosphate is labelled with an asterisk and a yellow arrow. **b**, Ribbon–stick representation of the precursor HDV ribozyme, colour-coded as in **a**. Divalent metal ion, gold. **c**, Experimental electron-density map at the active site of the Sr^{2+}-bound C75U mutant precursor ribozyme, superimposed with the structural model. The 2.45 Å sigma A-weighted $2F_o - F_c$ map (contoured at 1σ) (blue) was calculated with the scissile phosphate and the −1 base omitted. An omit $F_o - F_c$ difference map (3σ, red) calculated from a 2.9 Å resolution $Ir(NH_3)_6^{3+}$-bound C75U ribozyme structure reveals a 'predominant' position of the −1 base. The anomalous difference density contoured at 6σ (magenta) around the Sr^{2+} ion is coincident with a ball-shaped density of 8σ in the $2F_o - F_c$ map. **d**, The active site configuration in the Sr^{2+}-bound C75U mutant precursor ribozyme. The Sr^{2+} is surrounded by the following ligands (with indicated coordination distances): O2 of U20 (3.2 Å), O4 of U75 (2.7 Å), phosphate of U23 (4.2 Å), O5′ of G1 (5.2 Å), phosphate of C22 (5.1 Å) and phosphate of U −1 (5.2 Å). For reference, the distance between the metal and the 5′-O of G1 is 4.3 Å in the Mg^{2+}-bound structure, consistent with water-mediated contact. The distance from the metal to O4 of U75 is 4.0 Å in the $Co(NH_3)_6^{3+}$-bound structure. The attacking 2′-OH of U −1 in its predominant conformation is 5.5 Å away from the N3 of U75. Occupancies of Mg^{2+}, Mn^{2+}, Sr^{2+}, Ba^{2+}, $Co(NH_3)_6^{3+}$ and $Ir(NH_3)_6^{3+}$ in the active site are ~0.5–1.0, whereas the anomalous difference signal of Cu^{2+} is not above background.

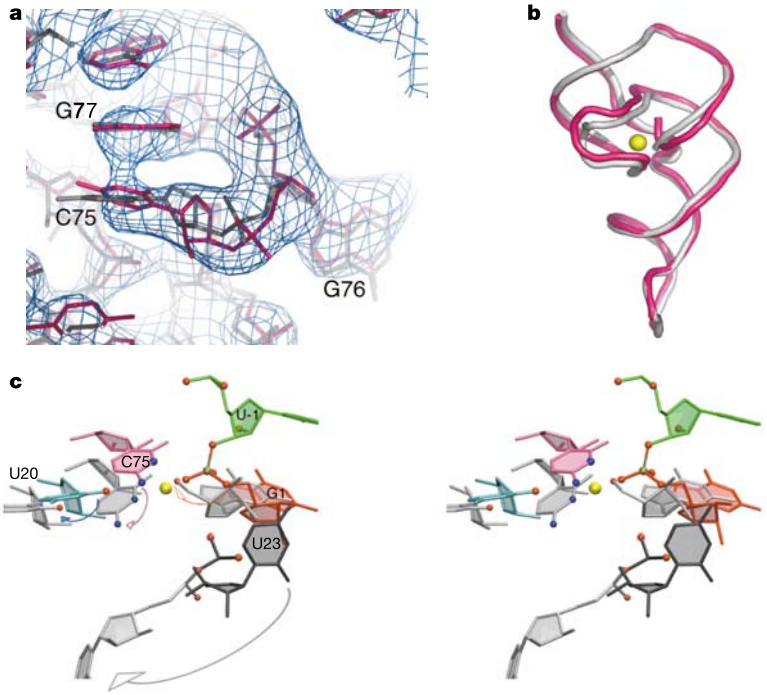

Figure 2 Conformational changes in the active site accompany HDV ribozyme cleavage. **a**, 3.4 Å experimental electron-density map of the wild-type precursor HDV ribozyme (1σ) superimposed on the refined wild-type structure model (magenta) and that of the C75U mutant (grey). **b**, Backbone alignment of the precursor (magenta) and product (grey) ribozyme structures. **c**, Stereo view of the aligned active sites of the precursor (coloured) and product (grey) ribozyme structures. Conformational changes were modelled using the C75U mutant ribozyme structure, shown by arrows.

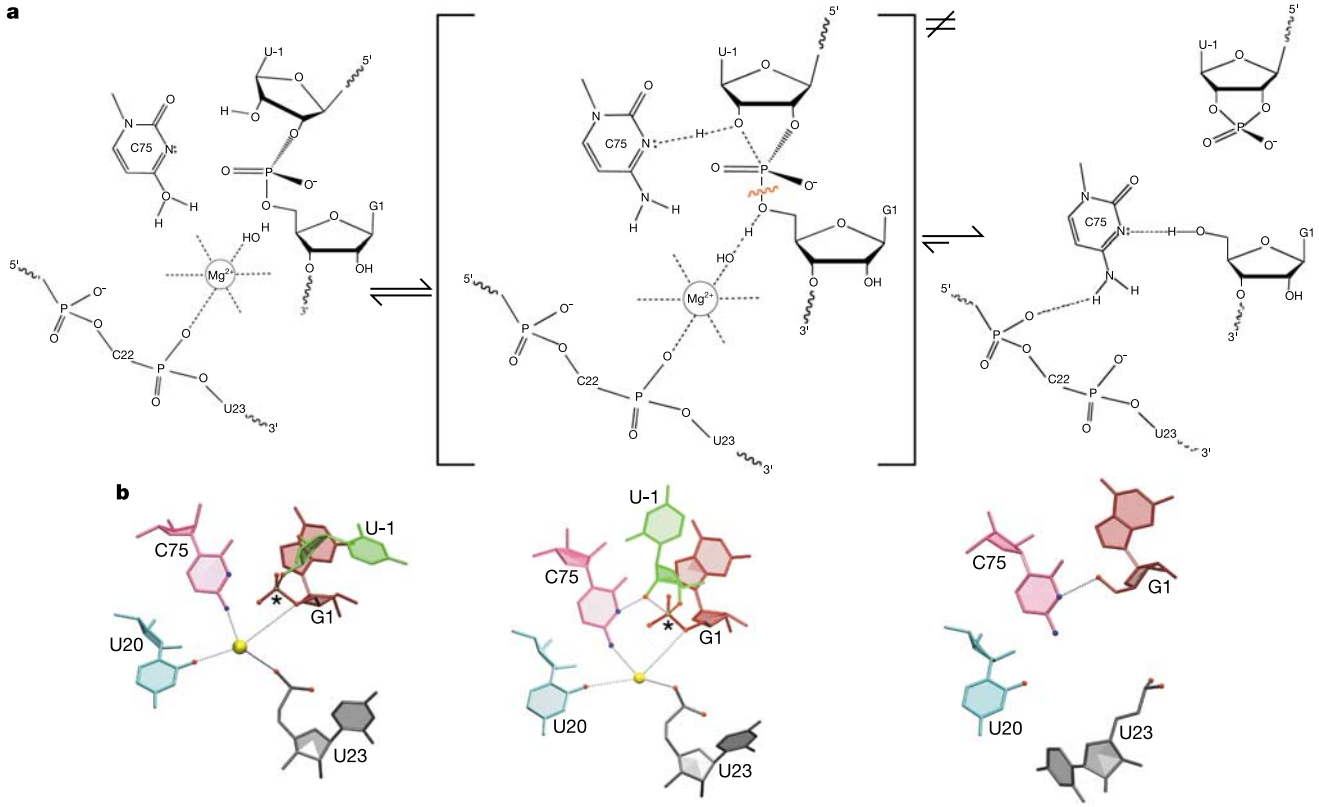

Figure 3 Proposed mechanism for general acid–base catalysis in the HDV ribozyme. **a**, In the ground state, a hinge rotation along O3′-P bond brings the nucleophilic 2′-OH to the in-line attack conformation. In the transition state, C75 (the general base) deprotonates the 2′-OH whereas the bound hydrated metal ion (the general acid) protonates the 5′ oxygen leaving group. Conformational changes after scissile bond breakage discharge the catalytic metal ion and down-shift the catalytic base C75 by 2 Å to enable hydrogen bonding with the 5′-OH of G1. **b**, Structural models of the HDV ribozyme in the ground state, transition state and product state. Some metal-chelating groups and coordinating waters are omitted for clarity.

zyme with and without divalent cations (Supplementary Fig. S1).

Strikingly, comparison of the precursor and product ribozyme structures reveals a significant local conformational change in the active site, resulting in dissociation of the catalytic metal ion after cleavage. Product–strand dissociation results in collapse of the P1 and P3 helices towards the centre of the ribozyme, pushing the ribose of the G1 base closer to C75 and deeper into the active site and closing off the binding site for the substrate strand. Removal of the scissile and the −1 phosphates upon product–strand dissociation triggers movement of the functional groups around the divalent cation (Fig. 2b, c). Furthermore, the C75 base shifts 2 Å deeper into the active site and forms a hydrogen bond with the 5′-OH leaving group.

It has been proposed that imidazole restores reactivity in HDV ribozymes with mutations at the active site C75 by supplying the missing general base functionality required to activate the 2′-OH nucleophile[10,11]. Although no imidazole-binding sites were observed in electron-density maps determined using diffraction data from imidazole-soaked C75U mutant crystals, the crystalline ribozymes undergo imidazole-induced self-cleavage without disrupting the crystal diffraction quality. In addition, C75U mutant ribozyme RNA was crystallized following incubation in an imidazole buffer solution for several days, avoiding any potential crystal lattice artefacts. The structures of these 'product' forms of the C75U mutant ribozyme (Supplementary Table S1) show that although the conformational change partially occurs and the catalytic metal ion dissociates, the U75 base does not move into position for hydrogen bonding with the 5′-OH. The importance of this motion and the resulting structural collapse of the product active site is emphasized by the fact that a U analogue with a pK_a near neutrality does not rescue ribozyme activity when substituted for U75[19]. The essential nature of the exocyclic amine of C75 can be explained by its requirement for stabilizing the active site conformational change that controls catalysis. These data point to an interesting parallel between the HDV ribozyme and pro-region-containing enzymes such as caspases, in which conformational changes induced upon cleavage of the inactive zymogen form of the enzyme stabilize the catalytic cleft[20]. Thus, in contrast to the hairpin and hammerhead ribozymes[21–24], the chemical step of the HDV ribozyme self-cleavage reaction is necessarily coupled to an active site rearrangement.

The precursor HDV ribozyme structures described above, together with previous biochemical data, are consistent with a model in which the sharply kinked RNA substrate is surrounded by two catalytic groups—a divalent metal ion coordinated through water to the 5′ oxygen of the leaving group and the C75 base positioned near the 2′-OH of the −1 ribose. The pK_a of C75 may be shifted to near-neutrality by the closely positioned scissile phosphate, enabling it to accept a proton efficiently from the attacking 2′-OH nucleophile. Such a pK_a shift would only be observed in the precursor ribozyme, where the scissile phosphate is present, and is consistent with the lack of a significant pK_a shift in the product form of the ribozyme[25]. The 2′-OH nucleophile in the ground-state conformation (Fig. 3, left) is 5.5 Å from the N3-H of U75 in the C75U mutant ribozyme structures and thus beyond hydrogen-bonding distance. It can be modelled within hydrogen-bonding distance of the U75 N3-H by a slight rigid-body rotation about the 3′-O–P bond of the −1 nucleotide. This rotated position brings the 2′-OH to the optimal in-line attack conformation (Fig. 3, middle), suggesting an additional role of C75 in the wild-type ribozyme in positioning the substrate. However, further rotation of U −1 to bring the 2′-OH near the metal ion results in steric clashes between the U −1 base and the P3 helix, leading us to conclude that the hydrated metal ion does not function as the general base in the reaction[12]. Instead, C75 acts as a general base in the transition state to activate the 2′-OH, whereas the hydrated metal ion acts as a general acid to stabilize the 5′ oxygen leaving group (Fig. 3). The proton transfer may occur in concerted steps in which a proton is shuttled from the 2′-OH to C75, to Mg(H_2O) through tautomerization, then to the 5′ oxygen, consistent with observed pH-rate profiles that argue against formal loss of a proton by the hydrated metal ion[11]. The conformational change in the active site following cleavage discharges the catalytic metal ion and displaces the C75 base such that the reverse (ligation) reaction is highly unfavourable (Fig. 3, right). Furthermore, closing of the space between the P1 and P3 helices blocks the binding site for the substrate strand. This explains why the HDV ribozyme is a dedicated nuclease and suggests that the virus evolved this unique catalyst to control the processing of replication intermediates during viral infection. □

Methods

RNA and protein preparation

Plasmids pL3 and pT3 encode the HDV wild-type and C75U mutant genomic ribozymes, respectively, with a U1A-binding site engineered in stem–loop P4[7], and a 3-nucleotide GAU sequence preceding the cleavage site. RNA was prepared by standard T7 polymerase run-off transcription using linearized plasmid and purified by denaturing gel electrophoresis. The wild-type precursor ribozyme RNA with a 2′-deoxy modification in the U −1 base was generated by DNA splint-mediated ligation[26]. Native and selenomethionyl-derivatized U1A-RDB proteins were produced as described previously[8].

Crystallization and diffraction data measurement

To obtain precursor ribozyme crystals, wild-type or C75U ribozyme RNA complexed with U1A-RBD protein at 0.5 mM concentration was diluted into nine volumes of denaturing buffer A containing 25 mM Tris-HCl pH 7.5, 20 mM NaCl, 2.5 mM $MgCl_2$ (replaced by 20 mM EDTA for the wild-type RNA) and 8 M urea. After overnight dialysis against this buffer, the complex was transferred in three 3-hour dialysis steps into buffer A containing 4 M, 2 M and 0 M urea, respectively, and reconcentrated to 0.5 mM. The wild-type ribozyme–U1A-RBD complex was crystallized by hanging drop vapour diffusion with a reservoir solution containing 5–10% (v/v) (±)-2-methyl-2,4-pentanediol (MPD), 50 mM sodium cacodylate pH 6.0, 40–80 mM NaCl, 20 mM EDTA and 5–15 mM spermine-HCl. The C75U mutant and the wild-type ribozyme with 2′-deoxy modification were crystallized in similar conditions or in the presence of 20 mM $MgCl_2$, $SrCl_2$ or $BaCl_2$ in place of EDTA. Structures of the C75U mutant ribozyme with Sr^{2+} or Ba^{2+} were determined from crystals grown in the presence of those ions. Mg^{2+}, Mn^{2+}, $Co(NH_3)_6^{3+}$, $Ir(NH_3)_6^{3+}$ and Cu^{2+} were introduced into the C75U ribozyme crystals by soaking in solutions containing 20 mM metal ion for 20 min, 30 min, 2 h, 6 h or overnight. The wild-type and mutant ribozyme RNAs in the crystals were confirmed to be in the precursor form by dissolving crystals after diffraction data collection and analysing the RNA on a 10% urea–polyacrylamide gel electrophoresis (PAGE). All crystals belonged to space group R32, with unit cell dimensions similar to those of the HDV product ribozyme crystals[7]. Native and anomalous diffraction data sets (near the absorption edge of the metal where possible) were measured for each of the metal-bound ribozyme crystal forms at beamlines 8.3.1, 8.2.1 and 8.2.2 at the Advanced Light Source (Supplementary Table S1) and processed using SCALEPACK2000[27].

Phase determination and structure refinement

The best phase information for the precursor ribozyme structure came from the Se-MAD (multi-wavelength anomalous diffraction) data set from a crystal of the C75U ribozyme mutant–selenomethionyl U1A-RBD complex. All four selenium sites were located using the program SOLVE[28]. Heavy-atom parameters were further refined using CNS[29], followed by density modification and phase extension to 2.3 Å against the Sr^{2+}-containing native data set. One $Ir(NH_3)_6^{3+}$ site was found and refined in the Ir-SAD (single-wavelength anomalous diffraction) data from a C75U mutant crystal soaked overnight in 1 mM iridium hexammine using SOLVE. Se- and Ir-phased electron-density maps were used to build the precursor HDV ribozyme model. The precursor ribozyme model was then used to perform molecular replacement using AMoRe (CCP4 suite[30]) on the rest of the native data sets. To determine the conformation of the cleaved C75U mutant ribozyme, the refolded C75U mutant ribozyme–U1A-RBD complex was dialysed against buffer A with 100 mM imidazole for 3 days; following this treatment, the crystallized complex was shown by urea–PAGE gel analysis to contain ~100% cleaved ribozyme. To test whether there were discrete imidazole-binding sites in the mutant ribozyme, crystals were soaked in buffer containing 100 mM imidazole for 1 h followed by diffraction data collection. No electron density corresponding to imidazole was observed in $2F_o - F_c$ and $F_o - F_c$ electron-density maps, consistent with the observation that the K_d of imidazole for the ribozyme is >1.2 M[10].

Refinement was carried out using CNS with 10% of the reflections removed for R_{free} factor calculation. Following rigid-body refinement, simulated annealing was performed on each refined structure to remove model bias. Ribozyme-bound metal ions were identified in anomalous difference electron-density maps. Alternating rounds of positional (Powell minimization), individual B-factor refinement and manual rebuilding were carried out until the R and R_{free} factors were below 30%. The sugar–phosphate density for the −1 base was clear at this stage for structures with resolution better than 2.6 Å. Together with the 'predominant' −1 base position density identified in the $Ir(NH_3)_6^{3+}$-bound ribozyme structure, the entire −1 base could be built into the precursor ribozyme structure with confidence. Although residual density is present, the −2 and −3 bases were omitted from the models, except for the Sr^{2+}-bound structure that contains the

−2 base. TLS[30] and REFMAC5 were used to further refine the Sr^{2+}- bound C75U mutant and wild-type ribozyme structures by modelling diffraction anisotropy.

Received 22 December 2003; accepted 23 March 2004; doi:10.1038/nature02522.

1. Shih, I. H. & Been, M. D. Catalytic strategies of the hepatitis delta virus ribozymes. *Annu. Rev. Biochem.* **71,** 887–917 (2002).
2. Rosenstein, S. P. & Been, M. D. Self-cleavage of hepatitis delta virus genomic strand RNA is enhanced under partially denaturing conditions. *Biochemistry* **29,** 8011–8016 (1990).
3. Reid, C. E. & Lazinski, D. W. A host-specific function is required for ligation of a wide variety of ribozyme-processed RNAs. *Proc. Natl Acad. Sci. USA* **97,** 424–429 (2000).
4. Suh, Y. A., Kumar, P. K., Taira, K. & Nishikawa, S. Self-cleavage activity of the genomic HDV ribozyme in the presence of various divalent metal ions. *Nucleic Acids Res.* **21,** 3277–3280 (1993).
5. Nakano, S., Proctor, D. J. & Bevilacqua, P. C. Mechanistic characterization of the HDV genomic ribozyme: assessing the catalytic and structural contributions of divalent metal ions within a multichannel reaction mechanism. *Biochemistry* **40,** 12022–12038 (2001).
6. Tanner, N. K. *et al.* A three-dimensional model of hepatitis delta virus ribozyme based on biochemical and mutational analyses. *Curr. Biol.* **4,** 488–498 (1994).
7. Ferre-D'Amare, A. R., Zhou, K. & Doudna, J. A. Crystal structure of a hepatitis delta virus ribozyme. *Nature* **395,** 567–574 (1998).
8. Ferre-D'Amare, A. R. & Doudna, J. A. Crystallization and structure determination of a hepatitis delta virus ribozyme: use of the RNA-binding protein U1A as a crystallization module. *J. Mol. Biol.* **295,** 541–556 (2000).
9. Oyelere, A. K., Kardon, J. R. & Strobel, S. A. pK(a) perturbation in genomic Hepatitis Delta Virus ribozyme catalysis evidenced by nucleotide analogue interference mapping. *Biochemistry* **41,** 3667–3675 (2002).
10. Perrotta, A. T., Shih, I. & Been, M. D. Imidazole rescue of a cytosine mutation in a self-cleaving ribozyme. *Science* **286,** 123–126 (1999).
11. Shih, I. H. & Been, M. D. Involvement of a cytosine side chain in proton transfer in the rate-determining step of ribozyme self-cleavage. *Proc. Natl Acad. Sci. USA* **98,** 1489–1494 (2001).
12. Nakano, S., Chadalavada, D. M. & Bevilacqua, P. C. General acid-base catalysis in the mechanism of a hepatitis delta virus ribozyme. *Science* **287,** 1493–1497 (2000).
13. Shih, I. & Been, M. D. Energetic contribution of non-essential 5′ sequence to catalysis in a hepatitis delta virus ribozyme. *EMBO J.* **20,** 4884–4891 (2001).
14. Pereira, M. J., Harris, D. A., Rueda, D. & Walter, N. G. Reaction pathway of the trans-acting hepatitis delta virus ribozyme: a conformational change accompanies catalysis. *Biochemistry* **41,** 730–740 (2002).
15. Harris, D. A., Rueda, D. & Walter, N. G. Local conformational changes in the catalytic core of the trans-acting hepatitis delta virus ribozyme accompany catalysis. *Biochemistry* **41,** 12051–12061 (2002).
16. Perrotta, A. T. & Been, M. D. A pseudoknot-like structure required for efficient self-cleavage of hepatitis delta virus RNA. *Nature* **350,** 434–436 (1991).
17. Jeong, S., Sefcikova, J., Tinsley, R. A., Rueda, D. & Walter, N. G. Trans-acting hepatitis delta virus ribozyme: catalytic core and global structure are dependent on the 5′ substrate sequence. *Biochemistry* **42,** 7727–7740 (2003).
18. Pyle, A. M. Metal ions in the structure and function of RNA. *J. Biol. Inorg. Chem.* **7,** 679–690 (2002).
19. Oyelere, A. K. & Strobel, S. A. Site specific incorporation of 6-azauridine into the genomic HDV ribozyme active site. *Nucleosides Nucleotides Nucleic Acids* **20,** 1851–1858 (2001).
20. Chai, J. *et al.* Crystal structure of a procaspase-7 zymogen: mechanisms of activation and substrate binding. *Cell* **107,** 399–407 (2001).
21. Rupert, P. B. & Ferre-D'Amare, A. R. Crystal structure of a hairpin ribozyme-inhibitor complex with implications for catalysis. *Nature* **410,** 780–786 (2001).
22. Rupert, P. B., Massey, A. P., Sigurdsson, S. T. & Ferre-D'Amare, A. R. Transition state stabilization by a catalytic RNA. *Science* **298,** 1421–1424 (2002).
23. Murray, J. B., Dunham, C. M. & Scott, W. G. A pH-dependent conformational change, rather than the chemical step, appears to be rate-limiting in the hammerhead ribozyme cleavage reaction. *J. Mol. Biol.* **315,** 121–130 (2002).
24. Dunham, C. M., Murray, J. B. & Scott, W. G. A helical twist-induced conformational switch activates cleavage in the hammerhead ribozyme. *J. Mol. Biol.* **332,** 327–336 (2003).
25. Luptak, A., Ferre-D'Amare, A. R., Zhou, K., Zilm, K. W. & Doudna, J. A. Direct pK(a) measurement of the active-site cytosine in a genomic hepatitis delta virus ribozyme. *J. Am. Chem. Soc.* **123,** 8447–8452 (2001).
26. Moore, M. J. & Query, C. C. Joining of RNAs by splinted ligation. *Methods Enzymol.* **317,** 109–123 (2000).
27. Otwinowski, Z. & Minor, W. Processing of x-ray diffraction data collected in oscillation mode. *Methods Enzymol.* **276,** 307–326 (1997).
28. Terwilliger, T. C. & Berendzen, J. Automated MAD and MIR structure solution. *Acta Crystallogr. D Biol. Crystallogr.* **55,** 849–861 (1999).
29. Brunger, A. T. *et al.* Crystallography and NMR System: A new software suite for macromolecular structure determination. *Acta Cryst. D.* **54,** 905–921 (1998).
30. Collaborative Computational Project, The CCP4 Suite: Programs for protein crystallography. *Acta Crystallogr. D.* **50,** 760–763 (1994).

Supplementary Information accompanies the paper on **www.nature.com/nature**.

Acknowledgements Diffraction data for this study were measured with the guidance of C. Ralston, J. Holton and co-workers. We thank M. Been, K. Karbstein, J. Piccirilli, R. Spanggord and N. Walter for comments on the manuscript and for sharing unpublished data. This work was supported in part by the NIH.

Competing interests statement The authors declare that they have no competing financial interests.

Correspondence and requests for materials should be addressed to J.A.D. (doudna@uclink.berkeley.edu). The atomic coordinates and structure factors have been deposited in the RCSB Protein Data Bank with accession codes 1SJ3 (C75U/Mg^{2+}), 1VBY (C75U/Mn^{2+}), 1SJF (C75U/$Co(NH_3)_6^{3+}$), 1SJ4 (C75U/Cu^{2+}), 1VBX (C75U/EDTA), 1VBZ (C75U/Ba^{2+}), 1VC0 (C75U/Sr^{2+}/Imidazole), 1VC6 (C75U Cleaved Product), 1VC7 (C75U/Sr^{2+}) and 1VC5 (Wild Type).

corrigendum

Characterization of a common precursor population for dendritic cells

Gloria Martínez del Hoyo, Pilar Martín, Héctor Hernández Vargas, Sara Ruiz, Cristina Fernández Arias & Carlos Ardavín

Nature **415,** 1043–1047 (2002).

In this Letter, we characterized a common precursor population for dendritic cells (DCs) isolated from mouse blood by their capacity to generate all DC subpopulations present in mouse lymphoid organs after transfer into irradiated recipients, including $CD8^-$ and $CD8^+$ DCs, as well as $B220^+$ plasmacytoid DCs. Phenotypically, they were defined as $CD11c^+$ MHC class II^- $CD11b^+$ $B220^+$ $CD62L^+$. However, recent results from our laboratory (C.A., Beatriz León, Verónica Parrillas and G.M.d.H., unpublished work) indicate that, owing to a defect in the isolation method that was used, this common DC precursor population was highly contaminated by circulating NK cells, which express NK1.1 and DX5, display cytolytic activity and are devoid of DC-reconstitution potential when transferred into irradiated mice (C.A., unpublished results). Therefore, the cell population described in our original report comprised $CD11c^+$ $B220^+$ $CD62L^+$ $F4/80^-$ $DX5^+$ NK cells and a population of $CD11c^+$ $B220^-$ $CD62L^-$ $F4/80^+$ $DX5^-$ precursor cells with DC differentiation potential. Consequently, as the latter could potentially represent a heterogeneous population containing more than one DC precursor population, the proposed existence of the common DC precursors remains to be established. Experiments are underway to clarify this situation. □